IEEE Access
Multidisciplinary ⋮ Rapid Review ⋮ Open Access Journal

Received 10 February 2025, accepted 26 February 2025, date of publication 6 March 2025, date of current version 18 March 2025.

Digital Object Identifier 10.1109/ACCESS.2025.3548933

RESEARCH ARTICLE

Design and Characterization of an Atmospheric Pressure Dielectric Barrier Discharge Reactor for Potential Air Disinfection Applications

SILVIA G. SCALTRITI, ANDREA CRISTOFOLINI, AND GABRIELE NERETTI
Department of Electrical, Electronic and Information Engineering, University of Bologna, 40135 Bologna, Italy
Corresponding author: Gabriele Neretti (gabriele.neretti@unibo.it)

ABSTRACT Dielectric Barrier Discharge (DBD) technology is increasingly applied for disinfection purposes, primarily for surfaces and materials. However, its use in air disinfection is still relatively underexplored, with limited studies focusing on reactor optimization. This paper presents the design and characterization of a laboratory-scale DBD reactor, named Grid-like Air Plasma Sanitizer (GAPS), optimized for air treatment. The reactor features two grid-shaped electrodes positioned within a sealed container designed to create a serpentine channel for the airflow, enhancing the contact surface between treated air and produced discharge. The reactor is powered by a custom-designed power supply, based on a multilevel inverter architecture, for a total bipolar output of ± 1.2kV. The power supply generates a high-voltage square waveform with a peak of ± 1.2kV, a period of 8 μs and a rise time of 6kV/μs, promoting the formation of a strong non-equilibrium plasma for microbial inactivation. Electrical performance is characterized using both the Lissajous diagram and the equivalent circuit method, giving results in good agreement with eachothers. Furthermore, electrostatic FEMM simulations show details on the electric field intensity distribution and reactor capacitance. The GAPS produces a uniform and homogeneous plasma discharge under an air flow rate of 12.5LPM, without a significant increase in the reactor temperature, and a low specific power consumption of 0.014W/cm^2. These results show promising potential for the GAPS and lay the groundwork for future research, including biological experiments to assess its efficacy in air disinfection applications.

INDEX TERMS Dielectric barrier discharge, bioaerosol inactivation, electrical characterization, atmospheric pressure plasma technology, plasma discharges, CAP, NTP, LTP, air disinfection.

I. INTRODUCTION

In recent years, air quality has become an increasingly critical issue, especially in the aftermath of the COVID-19 pandemic, which highlighted the role of indoor air in the transmission of infectious diseases. This heightened awareness has driven advancements in air sanitization technologies, aiming to create safer indoor environments in schools, offices, healthcare facilities, and public transportation systems.

While conventional approaches such as high-efficiency particulate air (HEPA) filtration and ultraviolet germicidal irradiation (UVGI) have been extensively employed, each method has known limitations and often lacks robust evidence of effectiveness in reducing infectious diseases in real-world settings [1]. For instance, HEPA filters must be periodically replaced and can show reduced efficiency for very small particles, while UVGI systems may pose safety concerns if not properly shielded. Recent reviews have thoroughly compared the advantages and drawbacks of conventional technologies with emerging methods [2].

Among emerging technologies, atmospheric pressure non-thermal plasma (NTP) generated by Dielectric Barrier Discharge (DBD) has attracted significant attention in the biomedical field over the past few decades. While the fundamental principles of an NTP reactor have been understood for more than a century, their applications in industrial

The associate editor coordinating the review of this manuscript and approving it for publication was Yizhang Jiang.

© 2025 The Authors. This work is licensed under a Creative Commons Attribution 4.0 License.
For more information, see https://creativecommons.org/licenses/by/4.0/

and biomedical fields remain an active area of research, with continuous advancements expanding their potential [3]. In the context of sterilization and disinfection, NTP based technology presents highly promising results, indicating its potential as a future alternative to address current and upcoming challenges [4], [5], [6]. Among the various NTP reactor configurations, the DBD is the most widely used due to its homogeneous discharge, inherent electrical insulation, and energy efficiency, making it a dependable and reliable source for decontamination treatments [4].

Depending on the operative conditions, NTP produces a rich "cocktail" of reactive species, including reactive oxygen species (ROS) and reactive nitrogen species (RNS), electric fields, charged particles, and ultraviolet radiation (UVR), which have been shown to play pivotal roles in observed biomedical outcomes [7], [8], [9]. While the state of knowledge regarding plasma-generated agents is advanced, several subcellular and molecular mechanisms remain under debate or are not fully understood [10], [11]. Although multiple NTP reactor designs have demonstrated encouraging results for PBAs disinfection [5], [12], [13], [14], [15], [16], [17], the reactors described are often far from being optimized. Indeed, the precise inactivation pathways of cold plasma remain partially unclear, but various factors, such as gas composition, reactor geometry, electrode configuration, direct/indirect treatment and power supply, undoubtedly influence the antimicrobial efficacy.

Previous studies, including those by Friedman et al., suggest that direct interaction between contaminated air and the plasma discharge zone achieves higher disinfection efficiency compared to relying solely on long-living reactive species like ozone [18], [19]. This observation underscores the importance of reactor designs that maximize direct contact between bioaerosols and the plasma zone.

In this paper, we present the design and characterization of a novel atmospheric-pressure DBD reactor intended for air disinfection, named Grid-like Air Plasma Sanitizer (GAPS). As already mentioned, although various authors have reported successful biological results with similar plasma reactors, many of these studies have not focused on optimizing the interaction between PBAs and the plasma zone. To address this gap, we have paid particular attention to reactor geometry, electrode configuration, and airflow distribution, aiming to increase the electrode surface exposed to the air flow, thus increasing the direct exposure of microbes to the discharge. According to [19], this is expected to lead to an enhancement of the inactivation efficiency with respect to existing designs. Furthermore, as it is well established that pulsed power supplies achieve superior performance compared to AC sources [20], a dedicated pulsed power supply was implemented to enhance the non-equilibrium nature of the plasma. The custom-built power supply, specifically tailored for the GAPS, was developed to operate at relatively low voltages, requiring only 1.2 kV peak, thanks to the selection of dielectric materials and optimized thickness. The focus of this paper is on engineering aspects, including the design, electrode configuration, electrical characterization, and fluid flow, rather than on microbiological inactivation experiments and assessment. The corresponding biological tests are beyond the scope of this study and will be conducted and presented in future work. Our aim is to demonstrate that, based on established design principles and preliminary considerations, this GAPS holds potential for air disinfection applications.

II. DESIGN OF THE DIELECTRIC BARRIER DISCHARGE REACTOR (GAPS)

The Dielectric Barrier Discharge (DBD) reactor GAPS proposed in this study is specifically designed to maximize the interaction between the plasma and the treated airflow, ensuring efficient and uniform treatment. The geometry of the reactor directs the flow through a precisely engineered flow path, promoting consistent and prolonged exposure to the plasma discharge areas.

The GAPS features two grid-shaped electrodes made of stainless steel AISI 301, chosen for its resistance to ozone-induced corrosion and high humidity environments. The electrodes, designed at the *Plasma Technology Laboratory* (PTL) at the University of Bologna and fabricated by *Chimimetal* company through a chemical photo-etching process, exhibit precise and uniform patterns with an external diameter of $92mm$, $0.5\ mm$thick with a mesh size of $2mm \times 2mm$, and a wire spacing of $0.42\ mm$ (see Figure 1).

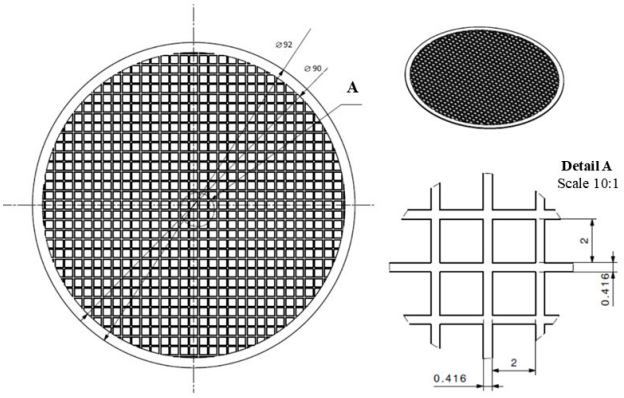

FIGURE 1. Technical drawing of the grid-shaped electrode: the 2D layout includes an isometric view of the electrode and a detailed close-up (A) highlighting the configuration of the grid structure.

One electrode is exposed while the other is coated with Rilsan® ES, a polyamide material widely used in the food industry due to its chemical resistance and high dielectric strength ($10kV/mm$ up to $100\mu m$ thickness). The coating was applied by *ZOCCA Coatings* company. The assembled GAPS is shown in Figure 2. Figure 2a, 2b and 2c are pictures of the real assembled DBD reactor captured from various perspectives. In Figure 2d the exploded CAD view highlights in the middle the two circular grid-shaped electrodes secured

in place by an external circular plexiglass structure. This structure not only holds the electrodes in alignment but also serves as a flow channel for the treated air. The upper circular plexiglass support aligns with the lower support, forming a sealed assembly through bolts and nuts. The CNC-machined airflow path in both the upper and lower plexiglass sections creates a controlled flow passage, designed as a serpentine channel throughout the grid mesh, where the flow traverses up and down multiple times, avoiding bypassing and ensuring consistent exposure of the treated fluid to the plasma discharge areas. This statement will be further validated by the CFD simulations presented later.

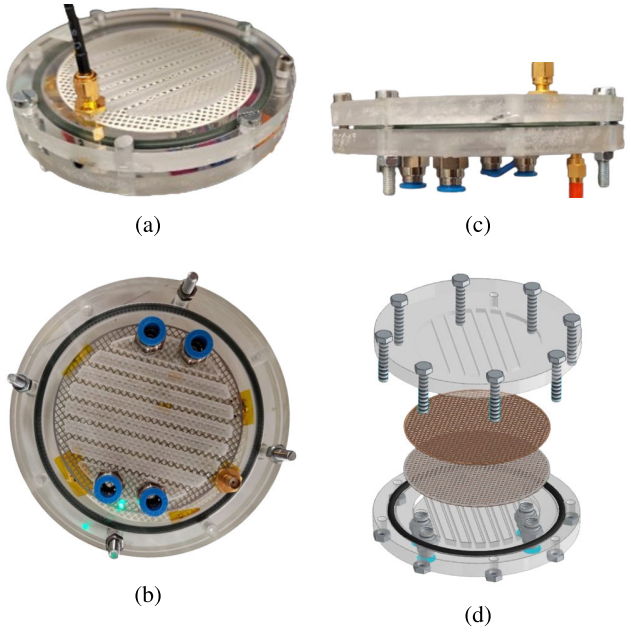

FIGURE 2. Photographs of the assembled GAPS reactor from the top view with one of the electrical connection (a), bottom view with the four quick-connectors for airflow (b), side view (c), and the exploded 3D CAD rendering created using SolidEdge software (d).

The two grid-shaped electrodes are differentiated by color in the illustration to indicate one as exposed (brown) and the other as coated with a dielectric material (white). A FKM (Viton) O-ring made of ozone-resistant material ensures a hermetic seal, preventing any leakage and safeguarding the system's integrity during operation.

The high-voltage and ground connections are embedded into the plexiglass body and are sealed with SMA airtightness connectors. Finally, the reactor incorporates four 6mm quick Festo connectors to enable the circulation of the gas flow through the system.

The GAPS operates in a surface dielectric barrier discharge (SDBD) configuration, where the plasma discharge occurs along the surface of the dielectric layer. This configuration allows for a hybrid plasma treatment, which includes both direct and indirect methods. This occurs because, within the reactor volume, the air interacts with the long-lived chemical species generated by the discharge, receiving an *indirect* treatment. Additionally, as the air passes multiple times through the grids where surface discharge occurs on the dielectric material, it also undergoes a *direct* plasma treatment. In this way, both long- and short-lived oxidizing species can contribute to the disinfection effect of the proposed GAPS device.

The power supply used to drive the GAPS was designed to provide an alternating voltage, essential for igniting and sustaining plasma formation, in particular a micropulsed bipolar voltage waveform. Its architecture is based on a pre-existing 49-level multilevel generator developed at the PTL [21], [22]. For this study, a 5-level cascaded H-bridge inverter was selected, consisting of 2 elementary units connected in series. Each elementary unit is capable of outputting $\pm 600V$ DC, to reach an alternating bipolar voltage of $\pm 1.2\ kV$, enough to enable the discharge on the dielectric surface. The coated electrode was connected to the high voltage terminal and the exposed one was grounded.

The multilayer generator enables fast rise time, approximately $6kV/\mu s$, allowing the system to reach high voltage levels within extremely short timescales, crucial for achieving efficient and homogeneous plasma conditions. The power supply, controlled via an Arduino microcontroller, enables the implementation of various waveform shapes. For this study, a bipolar square waveform is selected. In particular, a duty cycle characterized by an ON time of 8μs (one waveform voltage period) and an OFF time of 1000μs, proved to be the most effective in achieving homogeneous surface discharge while maintaining a low temperature environment. This characteristic facilitates the creation of a strongly non-equilibrium plasma, distinguished by a molecular and atomic excitation dynamic that differs significantly from that achieved with low-voltage excitation methods or slower rise times [23]. Furthermore, bipolar pulses were proven to be more efficient when the pulse duration is above $4\mu s$ [24]. The creation of a strong non-equilibrium plasma was proven by measuring the surface temperature of the GAPS by means of a FLIR T1020 infrared thermal camera, showing a maximum value of $29°C$ when no external airflow was passed through the reactor. The temperature is shown in Figure 3 where the photo was taken without the presence of quick-connectors to enable the camera to photograph the electrode surface under the reactor circular support, through the connector holes.

III. PHYSICAL CHARACTERIZATION OF THE REACTOR (GAPS)

This section describes the methods used for the physical characterization of the GAPS, focusing on both electrical and fluid dynamic analyses. The electrical characterization is focalized on the discharge power measurement which is a crucial parameter for the treatment efficiency evaluation. Meanwhile, the fluid dynamic characterization aims to enhance our understanding of the discharge-air contact behavior of the GAPS under treatment conditions (nominal flow).

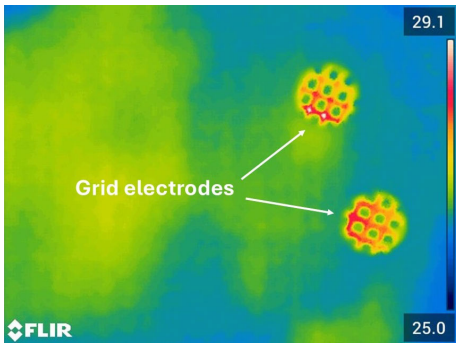

FIGURE 3. Temperature distribution on GAPS reactor surface with FLIR T1020 infrared-thermal camera. The photo was taken without the presence of quick-connectors to enable the camera to photograph the electrode surface under the reactor circular support, through the connector holes.

A. FLUID DYNAMICS CHARACTERIZATION

The fluid dynamics characterization of the GAPS was performed using Computational Fluid Dynamics (CFD) simulations, conducted on the cloud-based platform SimScale [25]. The main objective is to visualize the flow profile within the reactor under operational conditions, ensuring a uniform distribution of air flow for optimal plasma interaction. The volume simulated is obtained as the negative part of the 3D CAD of the GAPS modeled with SolidEdge [26], to simulate the empty spaces where the air is flowing, as shown in Figure 4c.

As already mentioned, GAPS geometry was designed to create a serpentine path across the grids, increasing the plasma treatment interaction volume for the incoming airflow. Air was modeled as the working fluid, with an inlet velocity of 8.3 m/s, which is derived from a volumetric flow rate of 12.5 LPM entering two inlet quick Festo connectors. These operating conditions pertain to experiments conducted for air disinfection treatment, which are not presented here. The boundary conditions included also an outlet at atmospheric pressure, as the experiment condition. A structured tetrahedral mesh containing 14 million nodes was created, with local refinements around critical areas (see Figure 4a and 4b). A mesh sensitivity analysis confirmed that further refinements did not significantly affect the results. The flow was modeled as an incompressible fluid in steady-state, with turbulence effects modeled using the k-omega SST turbulence model.

B. ELECTRICAL CHARACTERIZATION

Measurement of discharge power is not an easy task for non-sinusoidal waveforms, such as the micropulsed bipolar waveform used in this study [27], [28]. Two methods are employed to address this: the Lissajous figure method, or Q-V diagram, and the equivalent circuit method [29]. These approaches offer complementary insights into the power consumed by the GAPS, allowing for a more comprehensive evaluation of its efficiency.

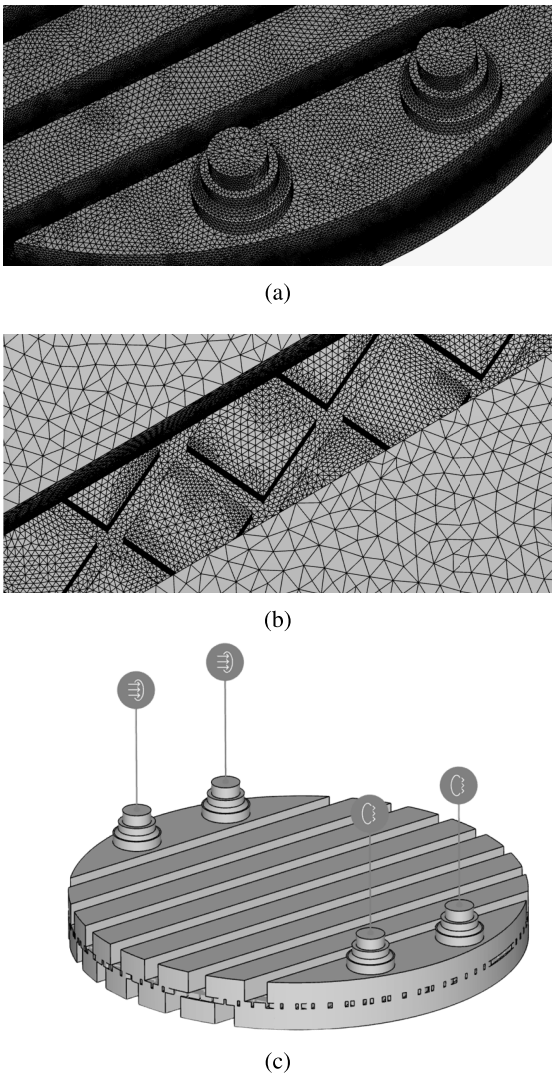

(a)

(b)

(c)

FIGURE 4. (a) Zoom of the mesh highlighting the inlet/outlet regions; (b) Zoom of the mesh around the critical points near the grid-shaped electrode. (c) 3D representation of the volume used as the domain for the 3D CAD simulation, representing the volume through which the flow passes.

1) EQUIVALENT CIRCUIT

The equivalent circuit method is based on the measurement of current and voltage applied to the reactor. The instantaneous power is calculated as $P(t) = v_m(t) \cdot i_m(t)$, and the average power is derived by integrating over the period of operation:

$$P_{\text{average}} = \frac{1}{T} \int_0^T v_m(t) i_m(t)\, dt \tag{1}$$

where T is the period of the voltage waveform, $v_m(t)$ is the measured voltage, and $i_m(t)$ is the measured current. In this study, T is equal to 1008 μs being the sum of the ON and OFF period, as presented in the previous section. While this method does not require prior knowledge of the reactor's electrical parameters and provides a quantitative estimation of average power, it faces challenges, particularly in pulsed DBD systems due to the harmonic content that

can significantly affect the measurement. High-bandwidth equipment is necessary to resolve the fast microdischarges and the integration must be performed over exact multiples of the discharge period T to ensure reactive power contributions average to zero.

The equivalent circuit method gives more insight into how the energy is distributed and enables to find the plasma current component. The system under study is represented as a series combination of the dielectric capacitance C_d and the gas gap capacitance C_g, with the latter in parallel with a plasma impedance Z_g, treated as a black box [30]. This circuit is shown in Figure 5. The equivalent circuit allows the decomposition of the total current into the capacitive displacement current and the plasma discharge current, as shown by the following equation:

$$i_z(t) = i_m(t) - C_g \frac{dv_g(t)}{dt} \tag{2}$$

where $i_z(t)$ represents the plasma discharge current. However, the method requires accurate knowledge of the dielectric and gas gap capacitances, C_d and C_g, which can be difficult to determine for complex geometries due to edge effects and non-uniform fields. To address this, the capacitance C_{OFF} of the reactor in the non-discharging phase can be used as a measurable quantity, enabling an alternative expression for the discharge current:

$$i_z(t) = \frac{1}{1 - \frac{C_{\mathrm{OFF}}}{C_d}} \left(\frac{dQ(t)}{dt} - C_{\mathrm{OFF}} \frac{dv_m(t)}{dt} \right) \tag{3}$$

The capacitances C_d and C_{OFF} can be measured with the Q-V diagram, as explained in the next section.

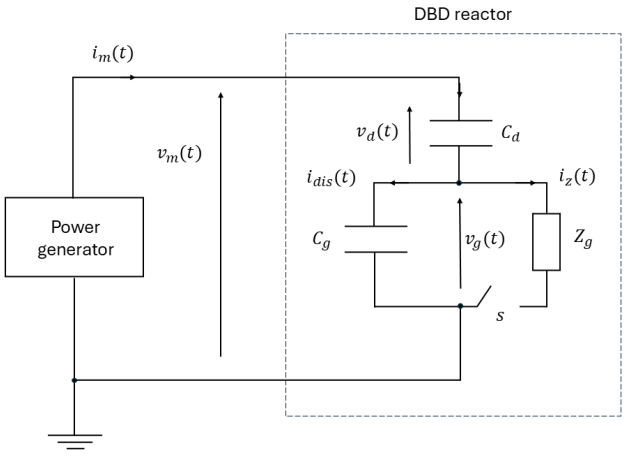

FIGURE 5. Equivalent circuit of the DBD reactor used for the analytical method.

2) Q-V LISSAJOUS DIAGRAM

The Lissajous figure method analyzes the charge-voltage ($Q-V$) characteristics of the reactor. These figures, obtained by plotting the instantaneous charge $Q(t)$ as a function of the instantaneous voltage $v_{\mathrm{m}}(t)$, are useful for diagnosing the electrical properties of the DBD reactor. The area enclosed by the $Q-V$ diagram corresponds to the energy delivered to the discharge and the average power can be defined as:

$$P_{\mathrm{average}} = \frac{1}{T} \int v_m(t)\, dQ(t) \tag{4}$$

where T is the period of the applied voltage. While sinusoidal waveforms produce quai-ideal parallelograms, deviations in the shape due to non-sinusoidal generators or real-world imperfections complicate interpretation. These deviations include almond, elliptical, noisy, or stepped shapes caused by partial discharging, plasma expansion, residual charge, electromagnetic interference, or discrete microdischarges. Despite these challenges, the Lissajous method requires only standard probes and provides a practical approach to power estimation. The Lissajous figure is obtained with a monitor capacitor C_m of 10 nF connected in series with the GAPS to capture the voltage $v_c(t)$ and subsequently estimate the transferred charge $Q(t)$. This capacitor value was chosen to balance between maintaining a high enough reactor voltage to initiate the discharge and minimizing noise in the capacitor signal. Q-V diagram can be used to obtain electrical information about the reactor. In fact, the slope of the Lissajous figures observed in the absence of discharge corresponds to the capacitance C_{OFF} and the slope at a saturation point can be seen as C_d [28]. This study found that results from the analytical and Lissajous methods were in good agreement, a favorable outcome given the typical discrepancies observed in pulsed supply DBD systems [31].

3) FEMM ELECTROSTATIC SIMULATION

FEMM (Finite Element Method Magnetics) is a well-established software package used to solve electromagnetic problems using the finite element method. In this research, FEMM was employed to perform electrostatic simulations focusing on a single *cell* area (see Figure 6b) of the GAPS composed of the two grid-shaped electrodes in contact with each other. By taking a cutting plane perpendicular to the grid and intersecting the midpoint of a single cell (dashed green line in Figure 6a and 6b we obtain a 2D representation of the electrodes. This includes the exposed electrode in contact with the dielectric and surrounded by air. Within a single cell, the plane intersects two parallel wires; if a half-cell is considered, it will feature only a single wire. Since the results shown no influence between the two wires distant 2 mm, in this paper only half-cell is presented, as in Figure 6d. The software was used to obtain the electric field distribution and potential gradients within the GAPS. Additionally, FEMM served to qualitatively assess the capacitance of the DBD reactor, through the simulation of an extruded single cell over the length of both sides, multiplied by the number of cells present.

The 2D electrostatic model simulated in FEMM consists of one electrode coated with Rilsan dielectric material ($\epsilon_r = 3.9$), depicted as an embedded square, and one exposed electrode. The exposed electrode was analyzed in two

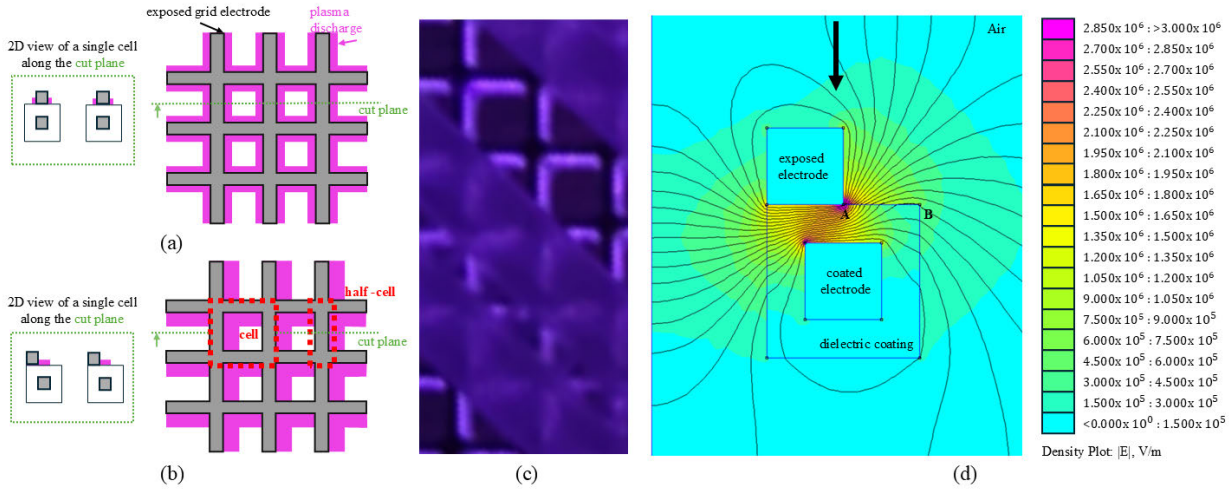

FIGURE 6. Illustrative figure of the conditions selected for the FEMM electrostatic simulation. (a) Representation of the aligned configuration of the two electrodes, shown both from above (right) and as a 2D view on a cut plane (left). (b) Representation of the misaligned configuration of the two electrodes, shown both from above (right) and as a 2D view on a cut plane (left). (c) Close-up view of the discharge from above in the misaligned configuration. (d) 2D model used in the electrostatic simulation for the misaligned configuration.

configurations: one perfectly aligned with the coated electrode and one displaced. These configurations are intended to represent two realistic scenarios concerning the arrangement of grid-like electrodes, considering potential mechanical misalignments during GAPS assembly. In Figure 6a and b the two drawings represent the grids from a top view with the relative plasma discharge areas. These drawings show the interaction between the exposed electrode (visible on top) and the coated electrode (not visible, under the exposed electrode in the 2D view in Figure 6a and 6b on the left). Such misalignment mirrors actual conditions and can be attributed to mechanical factors associated with the assembly of the reactor itself (due to electrical connections that do not allow perfect alignment). For this reason, only the misaligned configuration is presented in this study. This statement is sub-stantiated by the fact that Figure 6c provides a detailed zoomed-in view of the plasma discharge (taken from Figure 6b) and the electrodes displaced configuration. In Figure 6d the 2D of the cut plane perpendicular to the grid used for the simulation is depicted, highlighting the different parts and materials that make up the half-cell. The black arrow shows the direction in which the discharge in Figure 6c is photographed. The dielectric layer is uniformly applied, extending 200 μm around the coated electrode. The mesh was refined in regions with higher electric field intensities, ensuring accurate representation of the electric field.

Capacitance measurements were performed using the formula for the energy stored in a capacitor, given by:

$$W_c = \frac{1}{2}CV^2 \tag{5}$$

Rearranging this formula provides the capacitance:

$$C = \frac{2W_c}{V^2} \tag{6}$$

where V is the applied voltage across the electrodes in volts and W_c is the energy in joules. The integral of the electric field energy density, $u = \frac{1}{2}\epsilon E^2$, over the volume of the capacitor is computed to determine the total stored energy W_c:

$$W_c = \int \frac{1}{2}\epsilon E^2 \, d\tau \tag{7}$$

where ϵ is the permittivity of the dielectric material, E is the electric field strength, and $d\tau$ is the differential volume element.

The simulation results, presented in Figure 6d, are obtained with an imposed potential of the coated electrode equal to 400V, to study the electrostatic configuration of the GAPS at the discharge initiation (see Figure 7, 8a and related description).

IV. RESULTS

A. POWER MEASUREMENTS COMPARISON

The physical characterization was performed at a nominal airflow rate of 12.5 LPM, corresponding to the operating conditions of laboratory experiments on contaminated air treatment. Results related with these biological experiments are not presented here, as they fall outside the scope of this paper.

Figure 7 shows the applied voltage $v_m(t)$ and current $i_m(t)$ time behavior. The numbers 1 to 6 represent particular applied voltage values useful for the analysis of the Lissajous figure reported in Figure 9. The measured current differs from zero only during the time intervals in which the applied voltage rapidly changes (i.e. three times for each voltage period). The presence of a current peak is not strictly related to plasma formation, because the measured current takes into account the displacement and plasma current components (see Figure 5). The use of the proposed equivalent circuit method allows to quantify these three current components.

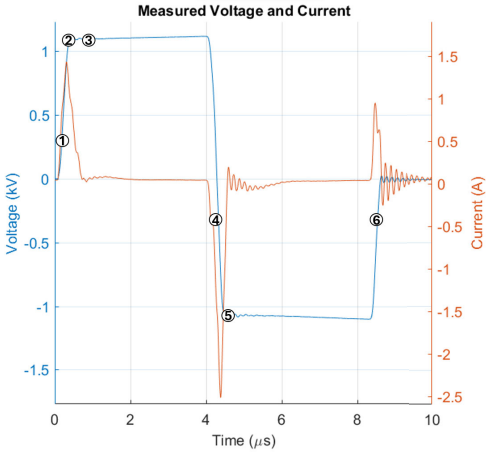

FIGURE 7. Microsecond bipolar power supply voltage waveform and GAPS reactor current waveform.

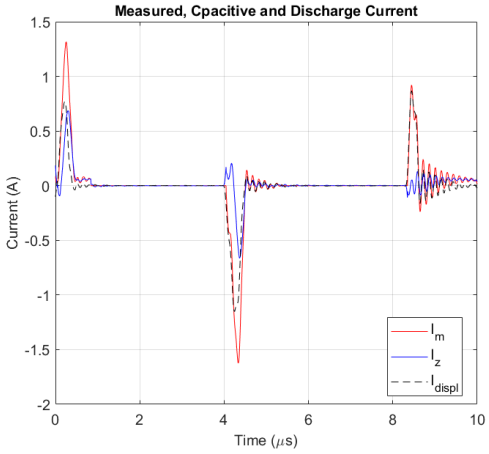

(a)

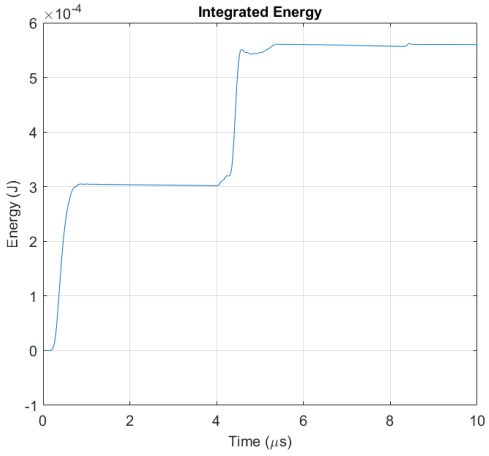

(b)

FIGURE 8. (a) Measured current profile and its components, displacement current and plasma current, obtained through equivalent circuit analysis. (b) Integrated energy.

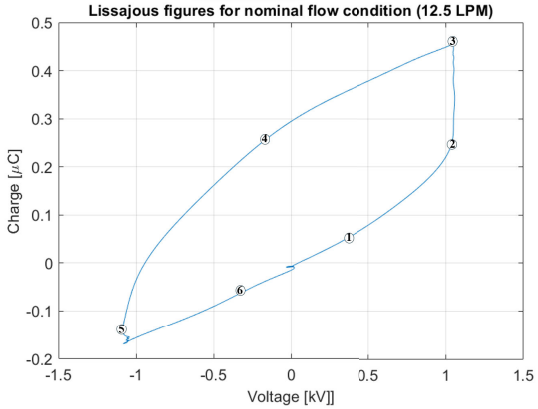

FIGURE 9. Lissajous figure acquired with the nominal flow (12.5 lpm) indicating points depicted in Figure 7.

Measured, displacement and plasma currents are shown in Figure 8a.

The plasma current $i_z(t)$ indicates that the discharge is ignited twice during the voltage waveform (during the first and the second voltage variation). Data presented in Figures 7 and 8a suggest that the discharge is initiated around $\pm 400V$ (points 1 and 4 in Figure 7). This observation of $400V$ as breakdown voltage will be further substantiated by the electrostatic analysis conducted using the FEMM software. The lack of a discharge in the last voltage steep variation means that the initiation requires an inversion of the electric field. In fact when transitioning from $+1.2\ kV$ to $0V$ or from $-1.2\ kV$ to $0V$ no discharge occurs. This behavior can also be seen by analyzing the integral energy associated with the measured current peaks, where the energy is delivered only during the first two voltage variations (Figure 8b). Its amount results to be the same during both discharge periods, being about $300\mu J$ each.

By plotting charge $Q(t)$ against $v_{DBD}(t)$ the Lissajous figure for the chosen operative condition is obtained, shown in Figure 9. The Lissajous figures illustrate the charge distribution during both positive and negative pulses, showing significantly more charge deposited during the positive pulse. This behavior is attributable to the enhancement effect, i.e., the increase in the electric field caused by positive charges accumulated during the first discharge. Conversely, the second discharge involves negative residual charges that are more mobile, resulting in reduced accumulation and influence on the local electric field during the plateau interval of the applied voltage. The residual charges deposited during each pulse, while not directly influencing discharge initiation (see FEMM results), modify the electric field behavior along decreasing voltage segments. This screening forced the voltage to be inverted before any discharge to happen.

A more comprehensive analysis of the phenomenon can be conducted by comparing the voltage and current with the Q-V diagram. In Figure 7 and 9 some crucial points are marked for a better understanding. Point (1) represents the first ignition at around $400V$. Point (2) represents the highest voltage value, positive peak, where the positive charge start to accumulate and lasts till point (3). After the second ignition (4) it is

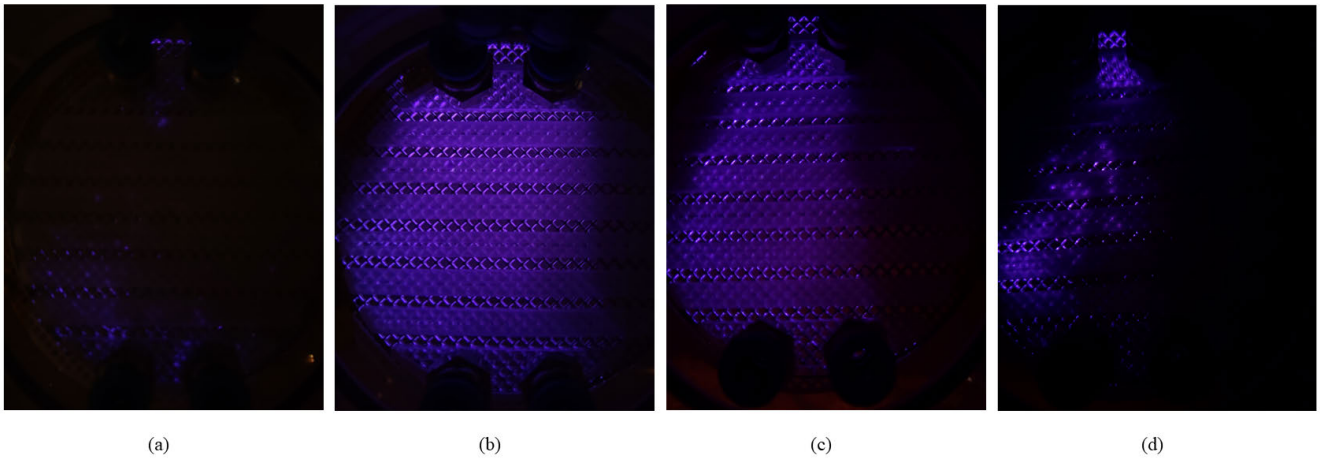

FIGURE 10. Photographs of the discharge taken with ISO 800 and a 20 s exposure under different operating conditions: (a) static conditions ($\dot{Q} = 0$); (b) nominal flow ($\dot{Q} = 12$ LPM, $t = 0$); (c) static conditions ($\dot{Q} = 0$, $t = 60$ s); (d) static conditions ($\dot{Q} = 0$, $t = 120$ s).

notable as there is no symmetrical charge accumulation with respect the positive voltage peak, and the discharge is faster and shorter (5). Point (6) denotes the $-400V$ voltage point that is not enough to initiate a discharge due to the charge shield, as explained above. It is worth noting that the experiments were repeated using both dry air and humid air at $70\%RH$, achieved with a BLAM nebulizer from CH Technology company, and no significant differences were observed in plasma uniformity or power consumption.

A peculiar behavior of the GAPS was observed during the transition from static conditions (no flow) to nominal flow conditions, and vice versa. As shown in Figure 10, under static conditions, the discharge is no longer homogeneous and instead covers only a limited portion of the reactor surface. Conversely, when the flow is activated at the nominal rate, the discharge ignites instantaneously and spreads over the majority of the dielectric surface. When the flow is turned off, the discharge does not immediately extinguish but gradually transitions back to static conditions, undergoing a progressive plasma extinction phase. A possible explanation of this phenomenon, is the presence of free charges able to shield the applied voltage. Whitout the external airflow, these charges can be accumulated onto the dielectric surface, enhancing their shielding effect. When the air is flushed into the sealed chamber, an higher amount of these generated charges are detached from the dielectric surface and mixed inside the GAPS. In this second scenario, a lower shielding effect is present.

The different working conditions of the reactor by varying the inlet airflow, were also studied by analyzing the power related to each configuration using both Lissajous figures and the analytical method. Measurements were taken at specific time points: static condition (no flow), nominal flow condition, and after increasing times from the flow extinction (30s, 60s, 90s, 120s, and 160s). The results of these analyses are shown in Figure 11a and Figure 11b.

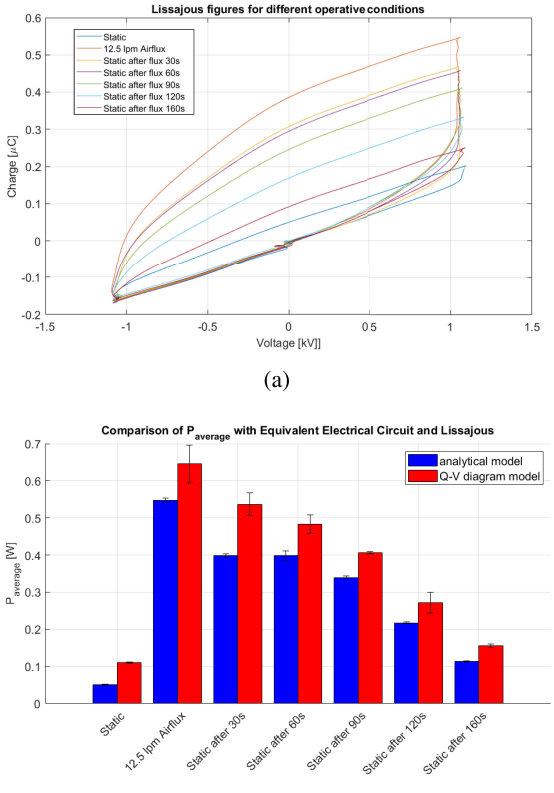

FIGURE 11. (a) Lissajous figures over time. The orange line represents the reactor under the nominal flow rate. Subsequent green, red, purple, teal and brown lines represent the reactor after the airflow is stopped (t=0) at 30s, 60s, 90s, 120s, and 160s, respectively. (b) DBD reactor average power, $P_{average}$, obtained with the equivalent electrical circuit analysis and with Lissajous figure in different operative condition: static, nominal airflow rate, after flux extinction at 30s, 60s, 90s, 120s, and 160s.

While these behaviors provide additional insights into the reactor's characteristics, they are not further investigated in

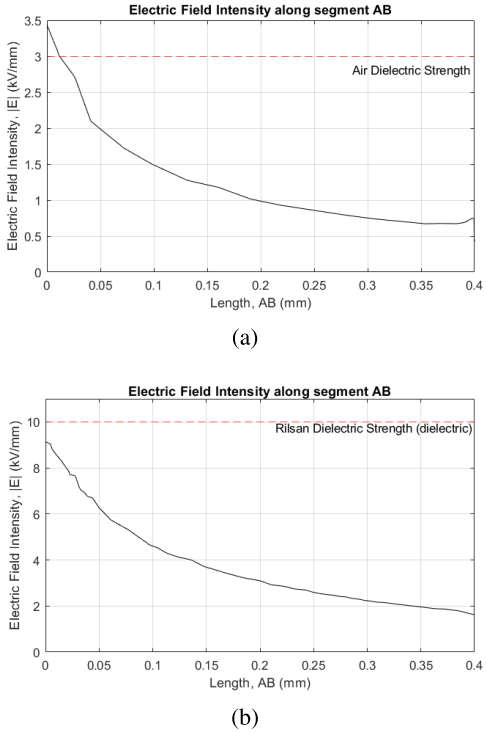

FIGURE 12. Trend of the electric field intensity along segment AB (see Figure 6d in two different electrostatic simulations: (a) 400 V, (b) 1200 V.

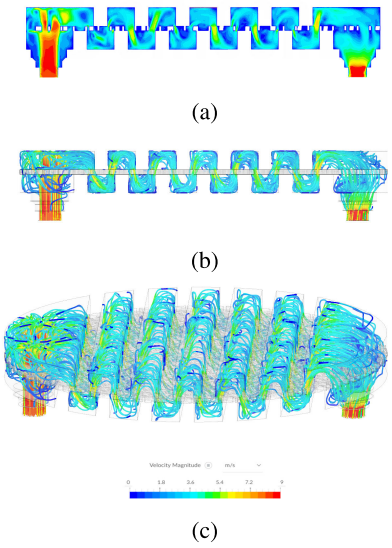

FIGURE 13. The velocity profile in a reactor section between inlet and outlet of the 3D CFD simulation performed with SimScale (a). Isometric view (c) and side view (b) showing the particle tracing results.

this study, as the primary focus remains on nominal flow conditions, used in the experiments. To validate the power measurements, results obtained via Lissajous figure analysis were compared with those derived from the analytical equivalent circuit method. Both approaches show consistent results, as illustrated by the bar graph in Figure 11b, although minor discrepancies are present due to experimental noise and systematic errors inherent in numerical differentiation and integration. Under nominal flow conditions, the reactor demonstrates stable discharge behavior with an average power of approximately 0.65 W, corresponding to a power density of 0.014 W/cm^2

B. FEMM RESULTS

The FEMM simulations yielded capacitance values of $500pF$ for the aligned electrode configuration (Figure 6a) and $150pF$ for the displaced configuration (Figure 6b). These values were in close agreement with experimental measurements. Notably, the actual configuration of the GAPS electrodes is displaced, as substantiated by the observed capacitance value of $147pF$, both with the Lissajous figure slope and the LCR meter measure, suggesting a robust correlation with the experimental data.

Figure 6d shows the electric field intensity and potential distribution for the displaced configuration when the high voltage terminal is subjected to a voltage of $400V$. The electric field is concentrated around the edges, where the exposed electrode meets the dielectric layer, with peak intensities occurring at the interface between the dielectric and air. These high-intensity regions are crucial for discharge initiation, as they exceed the dielectric strength of air (3 kV/mm), as evidenced by the results in Figure 12a. The intensity profile of the electric field ($|E|$) near the electrode is evaluated along the segment AB depicted in Figure 6d. In addition, simulations with the highest applied voltage of $1200V$ on the high-voltage electrode were conducted to evaluate the behavior under such extreme condition to prove the dielectric material reliability. As shown in Figure 12b, the electric field intensity remained within the dielectric withstand limit of Rilsan, which has a dielectric strength of up to $10kV/mm$ for thicknesses up to 100 μm. These simulation results correlate well with the observed plasma discharge and the associated electric field characteristics.

C. CFD RESULTS

The results of the CFD simulation, performed with SimScale software, are shown in Figure 13. Two views of the particle tracing results are presented, lateral (b) and isometric (c), in order to appreciate the homogeneity of the airflow distribution within the GAPS and, consequently, the optimization of the contact surface between the plasma and the air to be treated. The path that the air flux is forced to traverse is designed to make as many contacts as possible with the *direct* plasma discharge area, since it is known to be more efficient with respect to the *indirect* plasma treatment [18]. The path of the airflow can be clearly seen in Figure 13b, pointing out a quite homogeneous velocity in the whole reactor (13a). It is not easy to study the percentage of direct and indirect treatment in this geometry, due to the presence of the girds and the serpentine. CFD simulations were able to estimate the residence time which can be seen as the total treatment time in which the airflux experiences both treatments. This treatment

time was found to be 25*ms* for a single particle along the central path, from inlet to outlet. This time is very short, but in line with the results obtained in other studies where it has been proven sufficient to obtain good microbicidal results [12]. Despite this, the air is subjected to approximately 50 discharge events (two discharges in each cycle), allowing an intense treatment of the gas molecules.

V. CONCLUSION

The quality of air has become, in recent years, the subject of numerous studies aimed at improving air quality by inactivating microorganisms present in recirculated airflows and optimizing technologies dedicated to air disinfection. In this context, plasma technology is emerging as a valid alternative in the field of surface and liquid sterilization. However, its application to the treatment of airflows has not been extensively studied, nor has it been the focus of designing new reactors specifically for this purpose. To address this gap, this paper proposes a first prototype of a Dielectric Barrier Discharge (DBD) reactor, named Grid-like Air Plasma Sanitizer (GAPS), specifically designed for air treatment, optimizing the contact surface between the treated airflow and the discharge zones while maintaining low operating temperatures and minimal power requirements.

The results of the fluid dynamics simulation performed using SimScale demonstrate that the serpentine design ensures multiple passages of the airflow through the discharge zones. The temperature on the electrode surface does not exceed 30°C, and the power consumption under nominal flow rate conditions and maximum discharge surface is 0.65 W. Considering the plasma surface as the entire electrode in contact with the dielectric, the specific power is calculated to be 0.014 W/cm^2. The specific power is low compared to other air disinfection technologies and also compared to other plasma DBD reactor aimed for air disinfection. These results show promising potential for the proposed GAPS reactor and support future research for a scale up reactor designed for air disinfection applications and the relative biological experiments to assess its efficacy.

REFERENCES

[1] J. Brainard, N. R. Jones, I. C. Swindells, E. J. Archer, A. Kolyva, C. Letley, K. Pond, I. Lake, and P. R. Hunter, "Effectiveness of filtering or decontaminating air to reduce or prevent respiratory infections: A systematic review," *Preventive Med.*, vol. 177, Nov. 2023, Art. no. 107774.

[2] G. Berry, A. Parsons, M. Morgan, J. Rickert, and H. Cho, "A review of methods to reduce the probability of the airborne spread of COVID-19 in ventilation systems and enclosed spaces," *Environ. Res.*, vol. 203, Jul. 2021, Art. no. 111765.

[3] M. Laroussi, "A brief note on the history of the dielectric barrier discharge and its application for biological decontamination," *IEEE Trans. Radiat. Plasma Med. Sci.*, vol. 6, no. 1, pp. 121–125, Jan. 2022.

[4] K. E. Adesina, T.-C. Lin, Y. Huang, M. Locmelis, and D. Han, "A review of dielectric barrier discharge cold atmospheric plasma for surface sterilization and decontamination," *IEEE Trans. Radiat. Plasma Med. Sci.*, vol. 8, no. 3, pp. 295–306, Jan. 2024.

[5] H. Gao, G. Wang, B. Chen, Y. Zhang, D. Liu, X. Lu, G. He, and K. Ostrikov, "Atmospheric-pressure non-equilibrium plasmas for effective abatement of pathogenic biological aerosols," *Plasma Sources Sci. Technol.*, vol. 30, no. 5, Apr. 2021, Art. no. 053001.

[6] M. Laroussi, S. Bekeschus, M. Keidar, A. Bogaerts, A. Fridman, X. Lu, K. Ostrikov, M. Hori, K. Stapelmann, V. Miller, S. Reuter, C. Laux, A. Mesbah, J. Walsh, C. Jiang, S. M. Thagard, H. Tanaka, D. Liu, D. Yan, and M. Yusupov, "Low-temperature plasma for biology, hygiene, and medicine: Perspective and roadmap," *IEEE Trans. Radiat. Plasma Med. Sci.*, vol. 6, no. 2, pp. 127–157, Feb. 2022.

[7] N. T. Hiep, M. Nguyen, H. T. Nhut, N. T. Q. Hung, N. C. Manh, C. Lin, S. W. Chang, M. J. Um, and D.-H. Nguyen, "A review on sterilization methods of environmental decontamination to prevent the coronavirus SARS-CoV-2 (COVID-19 virus): A new challenge towards eco-friendly solutions," *Sci. Total Environ.*, vol. 904, Aug. 2023, Art. no. 166021.

[8] N. Kaushik, S. Mitra, E. J. Baek, L. N. Nguyen, P. Bhartiya, J. H. Kim, E. H. Choi, and N. K. Kaushik, "The inactivation and destruction of viruses by reactive oxygen species generated through physical and cold atmospheric plasma techniques: Current status and perspectives," *J. Adv. Res.*, vol. 43, pp. 59–71, Mar. 2023.

[9] T. Gerling, A. Helmke, and K.-D. Weltmann, "Relevant plasma parameters for certification," in *Comprehensive Clinical Plasma Medicine: Cold Physical Plasma for Medical Application*, 2018, pp. 43–70.

[10] Z. Chen, F. Bai, S. J. Jonas, and R. E. Wirz, "Cold atmospheric plasma for addressing the COVID-19 pandemic," *Plasma Processes Polym.*, vol. 19, no. 9, Sep. 2022, Art. no. 2200012.

[11] I. Niedźwiedź, A. Waśko, J. Pawłat, and M. Polak-Berecka, "The state of research on antimicrobial activity of cold plasma," *Polish J. Microbiology*, vol. 68, no. 2, pp. 153–164, Jan. 2019.

[12] T. Xia, A. Kleinheksel, E. M. Lee, Z. Qiao, K. R. Wigginton, and H. L. Clack, "Inactivation of airborne viruses using a packed bed non-thermal plasma reactor," *J. Phys. D, Appl. Phys.*, vol. 52, no. 25, Jun. 2019, Art. no. 255201, doi: 10.1088/1361-6463/ab1466.

[13] A. Bisag, P. Isabelli, G. Laghi, R. Laurita, G. Dirani, F. Taddei, C. Bucci, F. Capelli, M. Gherardi, A. Paglianti, V. Sambri, and V. Colombo, "Cold atmospheric plasma decontamination of SARS-CoV-2 bioaerosols," *Plasma Processes Polym.*, vol. 19, no. 3, Dec. 2021, Art. no. e2100133.

[14] L. Zhang, Y. Guo, X. Chang, Z. Yao, X. Wei, Z. Feng, D. Zhang, Q. Zhou, X. Wang, and H. Luo, "In-duct grating-like dielectric barrier discharge system for air disinfection," *J. Hazardous Mater.*, vol. 435, May 2022, Art. no. 129075.

[15] T. Xia, M. Yang, I. A. Marabella, E. M. Lee, B. A. Olson, D. Zarling, M. Torremorell, and H. L. Clack, "Inactivation of airborne porcine reproductive and respiratory syndrome virus (PRRSv) by a packed bed dielectric barrier discharge non-thermal plasma," *J. Hazardous Mater.*, vol. 393, Feb. 2020, Art. no. 122266.

[16] J.-S. Jung and J.-G. Kim, "An indoor air purification technology using a non-thermal plasma reactor with multiple-wire-to-wire type electrodes and a fiber air filter," *J. Electrostatics*, vol. 86, pp. 12–17, Jan. 2017.

[17] Y. Liang, Y. Wu, K. Sun, Q. Chen, F. Shen, J. Zhang, M. Yao, T. Zhu, and J. Fang, "Rapid inactivation of biological species in the air using atmospheric pressure nonthermal plasma," *Environ. Sci. Technol.*, vol. 46, no. 6, pp. 3360–3368, Mar. 2012.

[18] N. D. Vaze, M. J. Gallagher, S. Park, G. Fridman, V. N. Vasilets, A. F. Gutsol, S. Anandan, G. Friedman, and A. A. Fridman, "Inactivation of bacteria in flight by direct exposure to nonthermal plasma," *IEEE Trans. Plasma Sci.*, vol. 38, no. 11, pp. 3234–3240, Nov. 2010, doi: 10.1109/TPS.2010.2072788.

[19] M. J. Gallagher, N. Vaze, S. Gangoli, V. N. Vasilets, A. F. Gutsol, T. N. Milovanova, S. Anandan, D. M. Murasko, and A. A. Fridman, "Rapid inactivation of airborne bacteria using atmospheric pressure dielectric barrier grating discharge," *IEEE Trans. Plasma Sci.*, vol. 35, no. 5, pp. 1501–1510, May 2007.

[20] X. Lu, Z. Fang, D. Dai, T. Shao, F. Liu, C. Zhang, D. Liu, L. Nie, and C. Jiang, "On the chronological understanding of the homogeneous dielectric barrier discharge," *High Voltage*, vol. 8, no. 6, pp. 1132–1150, Oct. 2023.

[21] F. A. Dragonas, "Arbitrary waveform multilevel generator for high voltage high frequency plasma actuators," Ph.D. dissertation, Univ. Bologna, Bologna, Italy, 2014.

[22] C. A. Borghi, A. Cristofolini, G. Grandi, G. Neretti, and P. Seri, "A plasma aerodynamic actuator supplied by a multilevel generator operating with different voltage waveforms," *Plasma Sources Sci. Technol.*, vol. 24, no. 4, Jul. 2015, Art. no. 045018, doi: 10.1088/0963-0252/24/4/045018.

[23] E. Panousis, N. Merbahi, F. Clement, M. Yousfi, J.-F. Loiseau, O. Eichwald, and B. Held, "Analysis of dielectric barrier discharges under unipolar and bipolar pulsed excitation," *IEEE Trans. Dielectr. Electr. Insul.*, vol. 16, no. 3, pp. 734–741, Jun. 2009.

[24] J. R. Beveridge, S. J. MacGregor, J. G. Anderson, and R. A. Fouracre, "The influence of pulse duration on the inactivation of bacteria using monopolar and bipolar profile pulsed electric fields," *IEEE Trans. Plasma Sci.*, vol. 33, no. 4, pp. 1287–1293, Aug. 2005.
[25] GmbH. (2023). *Simscale*. Accessed: Dec. 4, 2023. [Online]. Available: https://www.simscale.com
[26] Siemens. (2023). *Solid Edge*. [Online]. Available: https://www.plm.automation.siemens.com/en/products/solid-edge/
[27] A. V. Pipa, T. Hoder, J. Koskulics, M. Schmidt, and R. Brandenburg, "Experimental determination of dielectric barrier discharge capacitance," *Rev. Sci. Instrum.*, vol. 83, no. 7, Jul. 2012, Art. no. 073506.
[28] A. V. Pipa and R. Brandenburg, "The equivalent circuit approach for the electrical diagnostics of dielectric barrier discharges: The classical theory and recent developments," *Atoms*, vol. 7, no. 1, p. 14, 2019.
[29] M. Hołub, "On the measurement of plasma power in atmospheric pressure DBD plasma reactors," *Int. J. Appl. Electromagn. Mech.*, vol. 39, nos. 1–4, pp. 81–87, Sep. 2012.
[30] M. Kuchenbecker, N. Bibinov, A. Kaemlimg, D. Wandke, P. Awakowicz, and W. Viöl, "Characterization of DBD plasma source for biomedical applications," *J. Phys. D, Appl. Phys.*, vol. 42, no. 4, Jan. 2009, Art. no. 045212.
[31] H. Jiang, T. Shao, C. Zhang, W. Li, P. Yan, X. Che, and E. Schamiloglu, "Experimental study of Q-V Lissajous figures in nanosecond-pulse surface discharges," *IEEE Trans. Dielectr. Electr. Insul.*, vol. 20, no. 4, pp. 1101–1111, Aug. 2013.

SILVIA G. SCALTRITI received the B.S. degree in energy engineering and the M.S. degree in electrical engineering from the University of Bologna, Bologna, Italy, in 2017 and 2020, respectively, and the second master's degree from NTNU. She is currently pursuing the Ph.D. degree in health and technology with the University of Bologna. During her second masters' year, she went to Trondheim, Norway, for Erasmus+ Exchange with NTNU.

From 2020 to 2021, she was a Research Assistant with the Department of Physics and Astronomy (DFA), Padua, Italy. From September 2023 to June 2024, she collaborated with the Swiss Plasma Center (SPC) Laboratory, EPFL, Lausanne, Switzerland. Her research interests include principally technological applications of dielectric barrier discharge (DBD) plasmas. Her work explores the use of DBD for medical sterilization applications, particularly for contaminated air disinfection. She is also involved into the development and optimization of high-voltage power supplies specifically tailored for DBD systems.

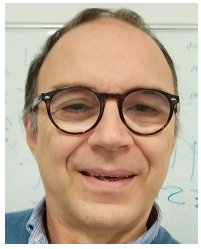

ANDREA CRISTOFOLINI was born in Catania, Italy, in January 1965. He received the Laurea degree in nuclear engineering and the Ph.D. degree in electrical engineering from the University of Bologna, Italy, in 1991 and 1995, respectively. In 1995, he joined the Department of Electrical Engineering, University of Bologna. Since 2001, he has been with the Department of Electrical, Electronic, and Information Engineering "Guglielmo Marconi," University of Bologna, where he is currently a Professor. He has been involved in various research projects concerning the MHD interaction in weakly ionized plasma for power generation and aerospace applications and the EHD interaction in barrier discharges. His research interests include numerical modeling and computational methods in electrical engineering.

GABRIELE NERETTI received the Ph.D. degree in electrical engineering from the University of Bologna, Italy, in 2009. Since September 2020, he has been an Associate Professor with the Department of Electrical Electronic and Information Engineering, University of Bologna. He published more than 60 international paper contributions and a book chapter, in 2016. His research interests principally include technological applications of non-thermal plasmas in aerospace and aeronautical domains and in the plasma medicine field. He is also involved in the design and realization of high voltage power supplies for plasma generation. He is a member of the International Society of Plasma Medicine and Editorial Board Member of the *Open Physics* and *Electronics* (MDPI).